

Sensitivity of the FCC-ee to decay of an axion-like particle into two photons

G. Polesello^a

^a*INFN Sezione di Pavia, Via Bassi 6, 27100 Pavia, Italy*

E-mail: giacomo.polesello@cern.ch

ABSTRACT: The decay of the Z boson into axion-like particles (ALP) at the Z -pole run of the proposed CERN FCC-ee collider is investigated. We perform a detailed study of final states with three photons or with a single photon and missing energy, yielding an evaluation of the accessible values of the ALP coupling to the photon for ALP masses between 0.1 and 85 GeV. Special attention is paid to the experimental implications of detecting the three-photon signature for the ALP mass region below 10 GeV. The FCC-ee run will be able to detect the ALP for couplings down to a few 10^{-3} TeV^{-1} over the considered mass range in an effective model where the ALP only couples to the $U(1)$ boson of the Standard Model.

Contents

1	Introduction	1
2	The model and its parameters	3
3	Signal and background generation	5
4	Detector simulation	6
5	Three-photon analysis	10
6	Monophoton analysis	15
7	Combined reach and Conclusions	17

1 Introduction

The next generation of high-energy particle colliders is under active discussion in the particle physics community. A very attractive option being discussed are e^+e^- circular colliders, such as the CERN FCC-ee [1]. These machines will provide access to a broad range of physics studies, from precision measurements of the Higgs boson and of Standard Model (SM) parameters, to direct searches for physics beyond the Standard Model (BSM).

A special strength of the program is the possibility of studying the production of new particles in a mass range of 100 MeV-100 GeV for extremely low values of their coupling to the Z boson exploiting the very large projected FCC-ee integrated luminosity at the Z -pole. These very low couplings can lead to long-lived particles decaying inside the detector (LLPs), allowing for searches with very low Standard Model backgrounds. This requires special care in the design of the detectors, and detailed studies are needed to understand the constraints imposed on the detectors by different final-state new physics signatures [2].

Of particular interest is the production of pseudoscalar axion-like particles (ALP, a in formulas), pseudo Nambu-Goldstone bosons which appear in theories where an approximate global symmetry of the theory is spontaneously broken. Such particles feature in several extensions of the Standard Model, and provide final-state signatures which can be explored at future colliders. Such signatures are discussed in detail in [3, 4] and [5, 6], based on effective models for the interactions of the ALP with SM particles.

The present study aims at evaluating the sensitivity for the production of such particles for the Z -pole run of the FCC-ee, with target integrated luminosity $L_{int} = 2.05 \times 10^8 \text{ pb}^{-1}$, distributed among the center-of-mass energies $\sqrt{s} = 88, 91, 94 \text{ GeV}$, corresponding to the production of approximately 6×10^{12} Z bosons. The ALP mass region ranging from 0.1

to 90 GeV is investigated, based on the model defined in [5, 6], for the process $e^+e^- \rightarrow Za$ followed by the decay $a \rightarrow \gamma\gamma$.

Preliminary studies for this process in the long-lived case are shown in [2] where the FCC-ee reach is given as a purely theoretical estimate of the number of produced events decaying inside a nominal detector volume. For the prompt decays, the study [7] addresses the Tera-Z option of the ILC, and it identifies the main experimental issues affecting the search.

The experimental reach of FCC-ee is assessed here based on a parametrised simulation of the proposed IDEA detector [8] and on the consideration of the leading irreducible backgrounds. This approach provides a realistic estimate of the physics coverage and valuable information on its dependence key elements of the detector performance. In the next paragraphs we will briefly comment on the limitations of the study, which will be addressed in the near future as the development of the FCC-ee detectors will converge towards the final design.

Two cases will be studied: in the first case the ALP decays inside the detector yielding a three-photon signature; in the second case the decays happens outside the detector, and the final state is a single photon and missing energy. For the decays inside the detector no distinction will be made between ‘prompt’ ALP decays, happening near the production point, and long-lived ones. The latter case requires a detailed study of the pointing performance of the electromagnetic calorimeter, which is not presently available. Likewise, for masses of the ALP below 1 GeV, and generically for long-lived ALPs, a good understanding of the shower position measurement and of the shower-shower separation of the electromagnetic calorimeter is needed. In the following, this will be replaced by parametrisations of the performance obtained from published simulation work by the calorimeter communities. A complete assessment of these performance aspects will require dedicated studies based on the GEANT4 simulation [9] of the full detector with 4π geometry, and the development of dedicated reconstruction algorithms.

Only irreducible backgrounds for the three-photon case are considered. Existing LEP studies give confidence that reducible backgrounds can be beaten down to a level well below the irreducible ones [10–13]. However given the extremely high Z statistics, this statement will need to be backed up by detailed detector studies.

The production of the ALP in the decay of the Z boson is addressed in this paper. An alternative production process, where the ALP is produced in the fusion of two photons radiated by the electron and the positron is studied in [14], and it is shown to cover a significant and complementary part of the parameter space.

The paper is organised as follows: the effective ALP model is first introduced and briefly discussed. In the following sections the Monte Carlo event generation is discussed, followed by a description of the adopted approach to detector simulation. On this basis two analyses are developed in the two following sections, addressing respectively the three-photon and the one-photon final state. Finally the additional coverage of FCC-ee with respect to existing searches is assessed for the studied benchmark model.

2 The model and its parameters

The present study is based on the ALP effective model described in [5, 6], which was also used in the previous FCC-ee study documented in [2].

The channel of interest for the Z -pole study is the decay of the Z boson into a photon and an ALP, followed by the decay $a \rightarrow \gamma\gamma$, yielding a three-photon final state, shown in Fig. 1.

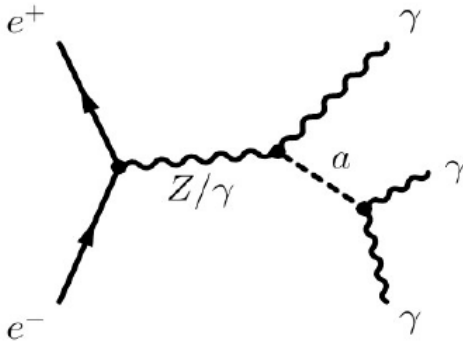


Figure 1. Feynman diagram for production and decay of the ALP at FCC-ee.

The part of the Lagrangian relevant to the production and decay of interest describes the coupling of the ALP to the photon and the Z boson after electroweak symmetry breaking as [6]:

$$\mathcal{L}_{\text{eff}} \ni e^2 C_{\gamma\gamma} \frac{a}{\Lambda} F_{\mu\nu} \tilde{F}^{\mu\nu} + \frac{2e^2}{s_w c_w} C_{\gamma Z} \frac{a}{\Lambda} F_{\mu\nu} \tilde{Z}^{\mu\nu} + \frac{e^2}{s_w^2 c_w^2} C_{ZZ} \frac{a}{\Lambda} Z_{\mu\nu} \tilde{Z}^{\mu\nu}. \quad (2.1)$$

where s_w and c_w are the sine and cosine of the weak mixing angle, Λ the new physics scale, and $F_{\mu\nu}$ and $Z^{\mu\nu}$ describe the photon, and Z boson in the broken phase of EW symmetry. The relevant Wilson coefficients $C_{\gamma\gamma}$, $C_{\gamma Z}$ and C_{ZZ} can be written as:

$$C_{\gamma\gamma} = C_{WW} + C_{BB}, \quad C_{\gamma Z} = c_w^2 C_{WW} - s_w^2 C_{BB}, \quad C_{ZZ} = c_w^4 C_{WW} + s_w^4 C_{BB}, \quad (2.2)$$

with C_{WW} and C_{BB} the Wilson coefficients for the coupling of the ALP to the unbroken SU(2) and U(1) gauge fields.

Following [6] we adopt a benchmark model where the tree-level couplings of the ALP to fermions and gluons are set to zero, and the ALP only couples to the U(1) gauge fields, i.e., the coefficient C_{WW} is set to zero. In this situation, from the formulas 2.2, $C_{\gamma Z} = -s_w^2 C_{\gamma\gamma}$, and the model is described by only two two parameters, the ALP mass m_a and $C_{\gamma\gamma}$. The branching ratio $BR(a \rightarrow \gamma\gamma)$ is 100%, and for $C_{\gamma\gamma} = 1$, and $\Lambda = 1$ TeV the cross-section at the Z pole is 2.7 pb for $m_a = 1$ GeV.

As only the $\gamma\gamma$ decay is open, the total width of the ALP is

$$\Gamma(a) = \frac{4\pi\alpha^2 m_a^3}{\Lambda^2} |C_{\gamma\gamma}^{\text{eff}}|^2 \quad (2.3)$$

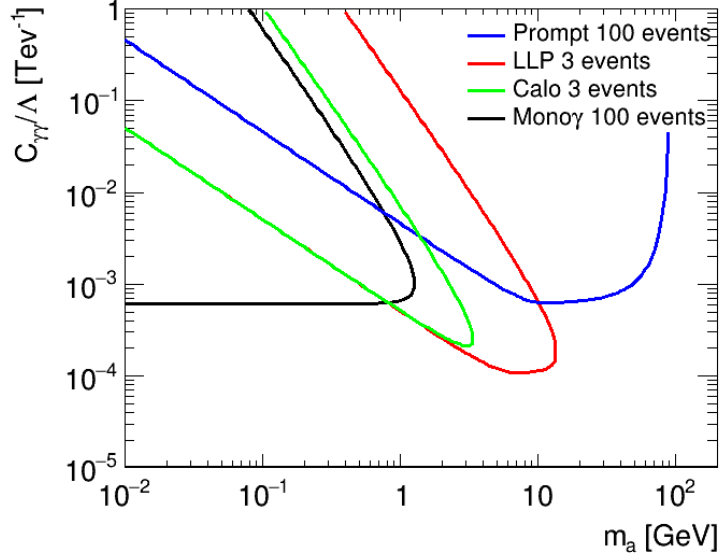


Figure 2. Areas in parameter space which can be addressed by different kinds of experimental ALP searches at the FCC-ee Z -pole run for the process $e^+e^- \rightarrow \gamma a \rightarrow 3\gamma$.

For sufficiently low values of m_a and $G_{\gamma\gamma}$ the ALP is long-lived, i.e. it has a measurable decay length L_a in the detector. As a guide to the experimental studies, it is useful to evaluate in the parameter space of the model how many ALP decays into two photons are expected for a statistic of 6×10^{12} Z -bosons, and in what region of this space they can be long-lived. The result is illustrated in Figure 2, and is classified in four regions:

- The ‘Prompt’ region, with $L_a < 1$ cm, where the path of the ALP in the detector does not affect the measurement of the kinematic properties. Since a large irreducible background is present for this case, consisting in the QED $e^+e^- \rightarrow \gamma\gamma\gamma$ process, the line bounding the region where at least 100 events are produced for the FCC-ee Z -pole run is shown.
- The ‘LLP’ region, where the ALP decays before reaching the calorimeter, and its path is in principle measurable, corresponding to $1 \text{ cm} < L_a < 200 \text{ cm}$ for the geometry of the IDEA detector. In this case no irreducible background is expected, and the curve for three events is shown.
- The ‘Calo’ region where the ALP decays inside the calorimeter, corresponding to $200 \text{ cm} < L_a < 400 \text{ cm}$. The signature is a prompt monochromatic photon recoiling against an energy deposition in the calorimeter. If it can be experimentally shown that the shower starts beyond the expected starting point of an electromagnetic shower in the calorimeter, this signal could also have no irreducible background, and the curve for three events is shown.

- The ‘Mono γ ’ region where the ALP decays outside the detector, yielding the signature of a prompt monochromatic photon recoiling against missing momentum. In this case the decay length requirement is $L_a > 450$ cm. The irreducible background for this channel is $e^+e^- \rightarrow \gamma Z, Z \rightarrow \nu\nu$, and the curve for 100 events is shown.

From Figure 2, the different approaches cover complementary areas in parameter space. The separation between ‘Prompt’ and ‘LLP’ relies on the experimental measurement of the impact angle of the photons on the calorimeter, which can be used to determine the position of ALP decay in the detector. This has been shown to be possible by the ATLAS Collaboration [15, 16], but, as discussed in the introduction, no study on the feasibility of this measurement and on the achievable measurement precision is available yet for the proposed FCC detectors. We will therefore develop a three-photon analysis where the ALP is required to decay at truth level inside the central detector, modelled as cylinder with radius 2 m and length 4 m, and no attempt is made to exploit the measurement of the impact angle of the detected photons. This analysis should cover both the ‘Prompt’ and the ‘LLP’ regions, and it will be referred to in the following as three-photon analysis. In addition we will perform a single-photon analysis addressing the ‘Mono γ ’ region.

3 Signal and background generation

The signal samples were generated with MG5aMC@NLO [17], based on the ALP_NLO_UFO UFO [6]. All the ALP couplings are set to zero except C_{BB} . This choice of parameters yields $C_{\gamma\gamma} = C_{BB}$, and a value of $C_{\gamma Z} = -s_w^2 C_{\gamma\gamma}$ which determines the production cross-section for the process of interest,

$$e^+e^- \rightarrow Z, Z \rightarrow \gamma a$$

The Λ suppression factor was set at 1 TeV. A scan was performed over the mass of ALP between 0.1 and 85 GeV, with $C_{\gamma\gamma} = 1$, and no lifetime simulation for the ALP. A total of 100k events per point were generated for these samples, which were used to study the kinematic selection for the prompt analysis. For masses below 10 GeV additional samples with simulation of the ALP lifetime for $C_{\gamma\gamma}$ between 5×10^{-4} and 5×10^{-2} and lifetime simulation were generated and used to study the impact of long ALP lifetimes on the analysis.

The LHE files were hadronised with PYTHIA8 [18] and then fed into the DELPHES [19] fast simulation of the IDEA Detector [8], based on the official datacards used for the "Winter2023" production of the FCC-PED study [20].

For the prompt analysis the irreducible background from the process

$$e^+e^- \rightarrow \gamma\gamma\gamma$$

was produced at LO with MG5aMC@NLO. The only generation-level requirements were that photons be produced within a pseudorapidity η of ± 2.6 . The cross-section for the process is 9.5 pb, and a sample of 10M events was produced, corresponding to approximately 1/200 of the expected statistics for the FCC-ee run at the Z pole. The events were then processed through the same PYTHIA8-DELPHES chain as the signal events.

For the monophoton analysis two background samples were likewise produced at LO with MG5aMC@NLO and processed through the PYTHIA8-DELPHES chain:

$$e^+e^- \rightarrow \gamma\nu\nu$$

and

$$e^+e^- \rightarrow \gamma e^+e^-$$

In both cases the matrix-element photon is required to be within $|\eta| < 2.6$ and to have an energy E_γ in a range around 45.5 GeV, which is the energy of the monochromatic photon for the ALP masses below 5 GeV, of interest for the monophoton signature. For the $\gamma\nu\nu$ samples two ranges were generated: $E_\gamma \in (44.5 - 46.5)$ GeV for a cross-section of 0.095 fb and $E_\gamma \in (40 - 50.5)$ GeV for a cross-section of 1.7 fb. For each sample 1M events were generated. The two samples are designed to provide adequate MC statistics for photon energy ranges compatible with the resolutions respectively of the crystal and fibre electromagnetic calorimeters. For the γe^+e^- sample the photon energy was required to be in the 40 – 50.5 GeV range, and the electrons were required to have pseudorapidity $|\eta| > 2.7$, yielding a cross-section of 0.016 pb. A million events were generated as well for this sample.

4 Detector simulation

The signatures under considerations involve events with only photons in the final state. Various aspects of the performance of the electromagnetic (EM) calorimeter determine the sensitivity of the analysis.

In particular, for ALP masses below ~ 10 GeV, the detection of the ALP decays depends on the precision with which the impact of each photon in the calorimeter can be measured. Moreover for low ALP masses, below $m_a = 1$ GeV the two photons for the ALP decay can be very collimated. The photon-photon separation power of the EM calorimeter, as well as the precision in mass reconstruction for two very collimated photons are essential performance figures for the ALP analyses. To model these effects, the DELPHES simulation was supplemented with dedicated parametrisations for the EM calorimeters, based on results from the detailed GEANT4 simulation of the calorimeter systems being proposed for the IDEA detector.

Two options are presently being considered for the electromagnetic calorimeter of IDEA, one based on a dual readout fibre calorimeter, and one based on scintillating crystals, with the latter being the baseline option.

For both options a geometry is assumed where the face of the calorimeter is modelled as a cylinder with 2 m radius and 4 m length, with the interaction point and origin of the coordinate system on the cylinder axis halfway between the two cylinder ends.

For the fibre option, the calorimeter is built as a matrix of steel tubes with 2 mm diameter, and inside each of them is located a fibre with 1 mm diameter. Each fibre is read out by a single SiPM, yielding lateral sampling of the electromagnetic shower with a granularity of 2 mm. No longitudinal segmentation is foreseen, but the arrival time of the

signal to the SiPM can be measured and used to study the longitudinal shower development. The performances of a prototype module with this geometry have been studied with a GEANT4 simulation. The most updated results are shown in recent talks by the HIDRA collaboration [21, 22], and are (E in GeV, x, y in mm):

- For the energy resolution:

$$\frac{\sigma(E)}{E} = \frac{0.139}{\sqrt{E}} + 0.006$$

- For the position resolution (in mm):

$$\sigma(x) = \frac{4.05}{\sqrt{E}} + 0.0; \quad \sigma(y) = \frac{3.23}{\sqrt{E}} + 0.0055$$

For the crystal option [23], the front face of the crystals has a nominal size of 1×1 cm, and the calorimeter is segmented in depth with a front crystal with nominal length 5 cm, and a rear crystal with nominal length 15 cm [24]. The following performance figures are assumed (E in GeV, θ in mm)

- For the energy resolution the value is taken from the DELPHES IDEA card, and is:

$$\frac{\sigma(E)}{E} = \frac{0.03}{\sqrt{E}} \oplus 0.005 \oplus \frac{0.002}{E}.$$

- The position resolution is quoted in [23] as:

$$\sigma(\theta) = \frac{1.5}{\sqrt{E}} \oplus 0.33;$$

when transformed in length coordinates on the cylinder surface, this yields a value similar to the one for the fibre calorimeter, but with a significantly higher constant term.

The simulation procedure starts from the selection of the truth photons produced by PYTHIA within $|\eta| < 2.6$, with the starting point inside the inner detector, and with an energy in excess of 100 MeV.

The θ and ϕ values of the intersection point of the momentum vector of the photons with the cylinder representing the calorimeter face are calculated, yielding the photon impact point in cylindrical coordinates. Thereafter the energy and the position of the impact point are smeared according to the resolution values given above.

In Figure 3 the resolution of the measured ALP mass is shown for the two different calorimeter designs. The results are shown for three ALP test masses, 0.2, 1 and 10 GeV, and in each plot the resolution obtained smearing both energy and impact position of the photon is compared to the one obtained smearing only the energy. At the very lowest mass considered the resolution is dominated by the impact point resolution, and is approximately the same for the two calorimeters. The contribution of the position resolution decreases for increasing masses, and is approximately negligible at 10 GeV.

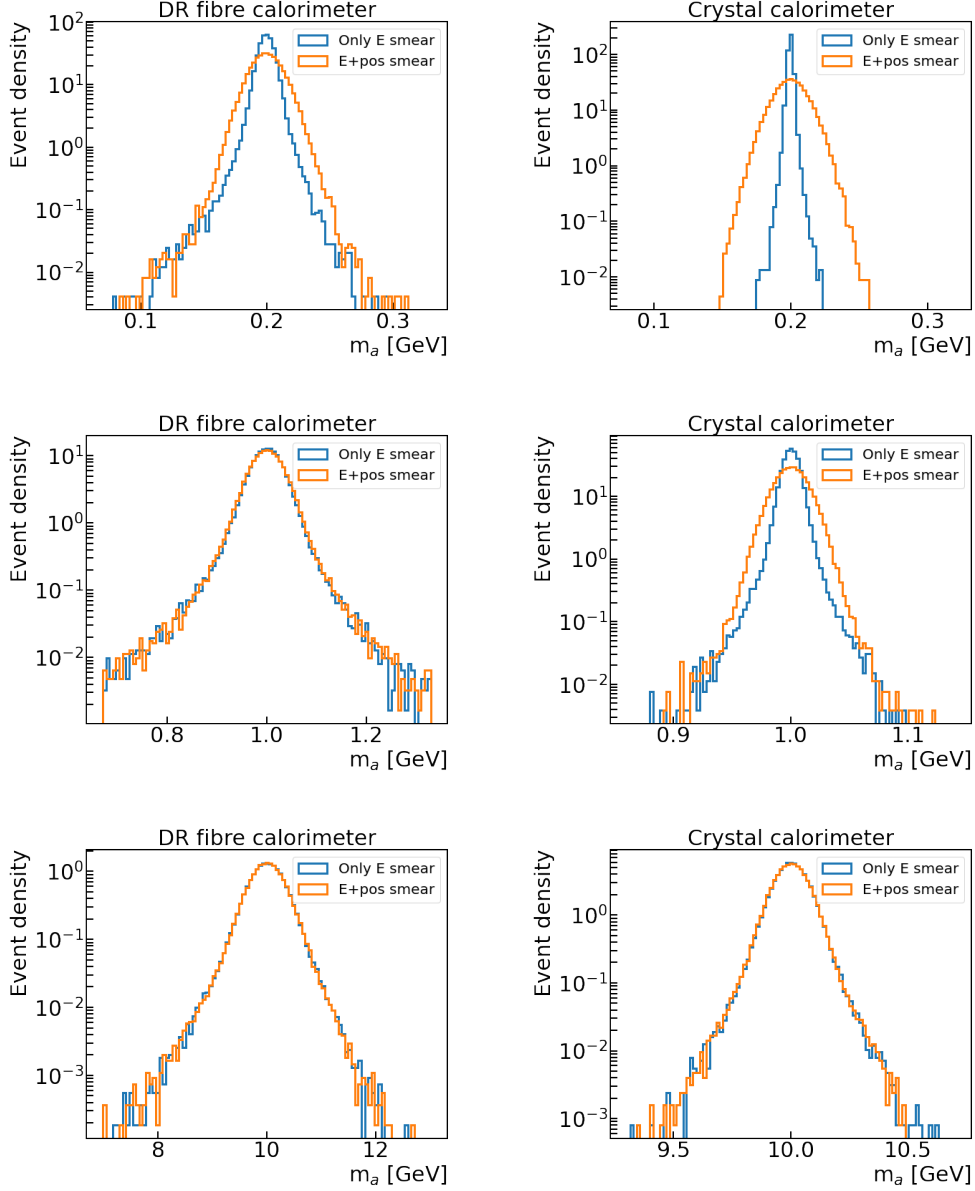


Figure 3. Reconstructed ALP mass for three different test masses: 0.2 GeV (top), 1 GeV (center) and 10 GeV (bottom). In the left (right) column the results for the fibre (crystal) EM calorimeters are shown. The blue line shows the resolution when only energy smearing is applied to the photons, the orange line when both energy and position smearing are applied.

Two additional issues affect the experimental sensitivity at low masses: the experimental merging of the two photons from the ALP decay, and the fact that, as discussed in the previous section, in part of the parameter space the ALP will have a measurable path in the detector before decaying.

The first issue is discussed in detail in [7] in the framework of an ILC analysis. The minimum distance in radians between two photons from the decay of a resonance of mass m_a and energy E_a is given by the formula

$$\Delta\alpha(\gamma\gamma) = 2 m_a/E_a,$$

yielding values of 0.004, 0.02, 0.04 radians for 0.1, 0.5 and 1 GeV respectively, which at a distance of 2 m from the decay point correspond to 0.8, 40 and 80 mm. If the distance between two showers is smaller than the Molière radius of the calorimeter, the two showers are not fully separated, which may mean that the two photons are seen as one, or that there is added uncertainty on the mass measurement from the uncertainty on the energy sharing between the two clusters.

Detailed simulations incorporating the detailed geometry of the calorimeter systems are needed to understand these effects. Thanks to the high granularity and the small Moliere radius (2.2 and 2.4 cm respectively for crystal and fibre) of the calorimeters under consideration, modern imaging techniques based on convolutional neural networks should allow photon-photon mass reconstruction down to values of m_a of ~ 0.1 GeV. This is demonstrated in an existing study based on the CMS calorimeter [25]. In that case a visible mass peak is obtained for $\gamma\gamma$ resonances with masses as low as 100 MeV, and transverse momenta in the range 30-55 GeV. Considering the higher granularity of the calorimeters under discussion for FCC, and the larger distance of the calorimeters from the interaction point, one can expect even better performance in the FCC case. For the present study, a sharp cutoff on the angular distance between the two photons from the ALP decay $\Delta\alpha$ is applied, and events with $\Delta\alpha$ below a given value are rejected in the analysis. The considered values of $\Delta\alpha$ are 0.01, 0.02, 0.03 radians, corresponding respectively to a distance between the two photons on the face of the calorimeter of respectively 2, 4 and 6 cm. The default value for the crystal calorimeter is taken as 0.02 radians, corresponding to four cells, and for the fibre calorimeter as 0.01 radians, corresponding to ~ 10 fibres.

The second effect to be considered is the impact of the long lifetime of the ALP on the measurement of the kinematics. The mass reconstruction algorithm assumes that the ALP decays in the center of the detector. The wrong angle between the two photons will thus be used in the invariant mass calculation, biasing the reconstruction of the ALP mass peak. The parametrised simulation described above describes this effect, as shown in Figure 4, where the reconstructed value of m_a is plotted for $m_a = 1$ GeV, and three different bins in the distance of the reconstructed vertex from the center of the detector, around zero, 500 and 1000 mm respectively. As expected, for the displaced vertexes the mass is reconstructed incorrectly, thus affecting the kinematic selections.

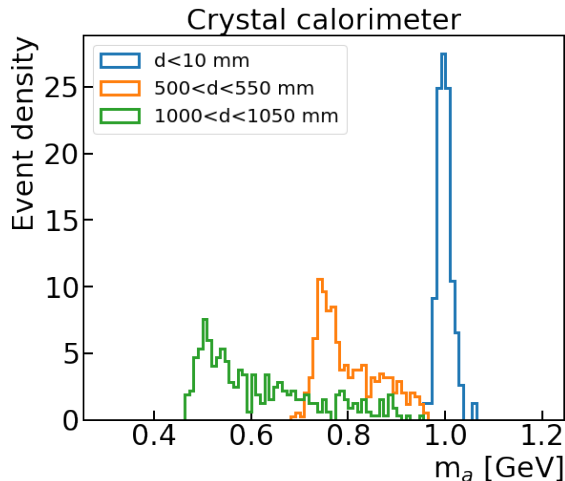


Figure 4. Reconstructed ALP mass for $m_a = 1$ GeV, and three different bins in the distance of the reconstructed vertex from the center of the detector, around zero (blue), 500 (orange) and 1000 (green) mm respectively. The crystal calorimeter configuration is shown.

5 Three-photon analysis

The final state for the process of interest involves three photons of which one is produced in the decay of the Z (γ_3) in the following, and two (γ_1 and γ_2) are produced in the decay of the ALP. The first step of the analysis consists in assigning each of the detected photons to one of the two classes.

If a specific test mass of the ALP, m_a is considered, the energy of the photon from the Z decay has a fixed energy E , determined by the recoil formula:

$$E = \frac{E_{CM}^2 - m_a^2}{2 E_{CM}} \quad (5.1)$$

Where E_{CM} is the center-of-mass-energy in of the collisions, 91.2 GeV for the present study.

Assume a test mass m_a , and the corresponding value of the recoiling photon E . For each event and for each of the possible three assignments of one of the detected photons as γ_3 , the variable M_{cut} can be built as:

$$M_{cut}^2 = \frac{(m_{\gamma_1\gamma_2} - m_a)^2}{\sigma(m_a)^2} + \frac{(E_{\gamma_3} - E)^2}{\sigma(E)^2} \quad (5.2)$$

Where the $\sigma(m_a)$ and $\sigma(E)$ are respectively the expected photon-photon mass resolution, and photon energy resolution. These values depend on the detector configuration and can be calculated from the simulation. The variable M_{cut} measures the compatibility of a given assignment with the expected signal kinematics.

The assignment which yields the minimum value for M_{cut} is taken as the correct one for the test mass m_a , and all the variables used in the analysis are calculated based on this assignment.

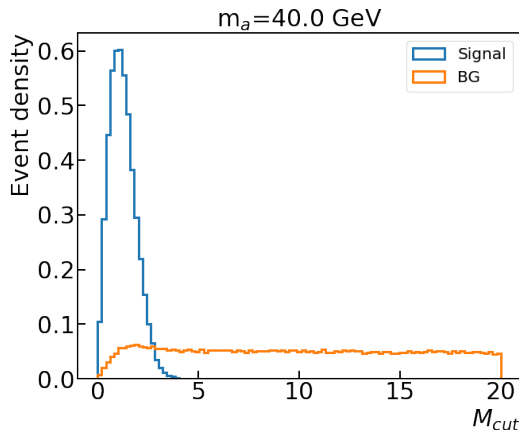


Figure 5. Distribution of the variable M_{cut} for signal (blue) and background (orange) for $m_a = 40$ GeV.

The variable M_{cut} is approximately independent of m_a , and of the studied calorimeter configuration, and has a good signal to background separation power. The distribution of M_{cut} , truncated at a value of 10 is shown for $m_a = 40$ GeV in Figure 5, for both signal and background. Besides the selection on M_{cut} , additional separation power between signal and background can be obtained through a detailed study of the angular distributions of the final state photons.

Each event is fully defined by 9 variables, i.e. the three-momenta of the photons. The energy and momentum constraints from the e^+e^- collision reduce the independent variables to five. The signal is a sequence of two-body decays, therefore a convenient choice of variables is the ALP mass built as the invariant mass of γ_1 and γ_2 , the θ and ϕ of the photon from the $Z \rightarrow \gamma a$ decay in the lab frame, and θ and ϕ of one of the photons from the $a \rightarrow \gamma\gamma$ decay, calculated in the rest frame of the ALP. Given the cylindrical symmetry of the system around the beam axis, the events can be rotated in such a way that $\phi_{\gamma_3} = 0$. After this rotation, the event is fully defined by $m_{\gamma_1\gamma_2}$ and by three angular variables. For the event selection we use $\cos \theta_{\gamma_3} = -\cos \theta_{ALP}$, $\cos \theta_{\gamma_1}$ and ϕ_{γ_1} where the latter two are calculated in the ALP rest frame. The distributions of the three angular variables are shown in Figures 6-8 for two different test masses and for both signal and background.

For the signal, since a is a scalar $\cos \theta_{\gamma_1}$ and ϕ_{γ_1} have a flat distribution, which is not the case for the background. For each test mass a signal selection is developed, based on the following steps:

- Events with exactly three photons within $|\eta| < 2.6$ and with energy $E_\gamma > 0.1$ GeV are selected, and for those events the photons are assigned to the desired ALP kinematics as described above.
- A preselection is applied, requesting that the invariant mass of the three leptons is above 84.5 (89.5) GeV for the DR calorimeter (crystal calorimeter) respectively. This cut has approximately 100% efficiency for signal, and rejects possible instrumental

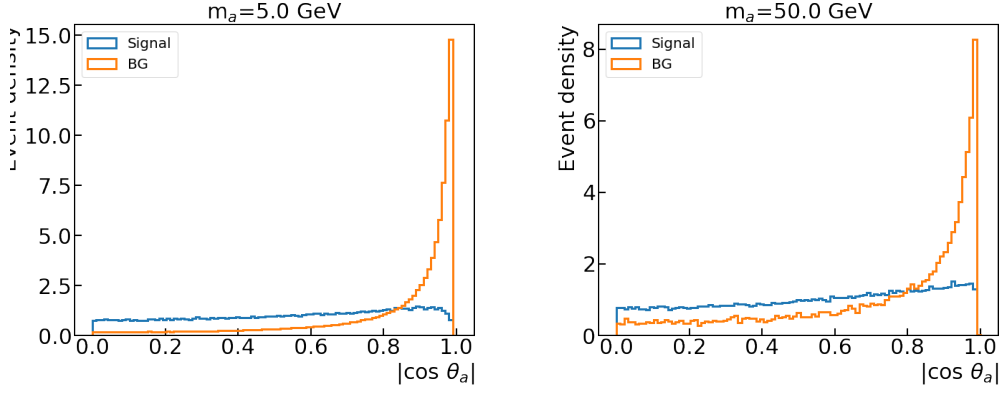


Figure 6. Distribution of the variable $\cos\theta_{ALP}$ for signal (blue) and background (orange) for two values of m_a , 5 (left) and 50 (right) GeV.

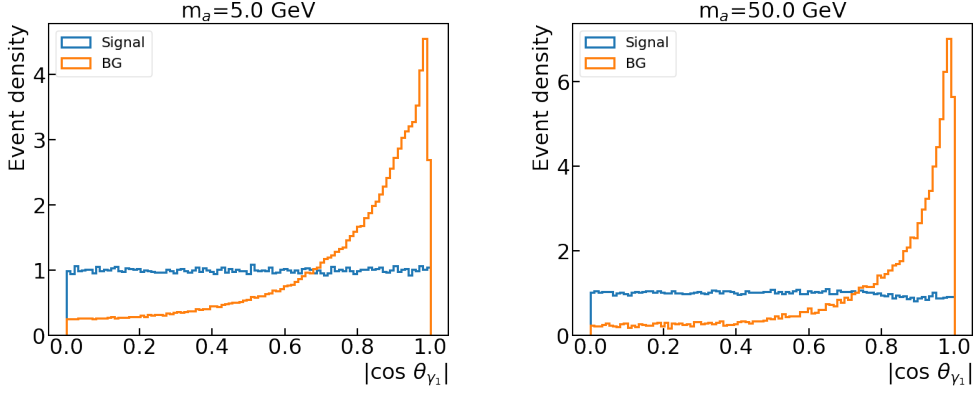


Figure 7. Distribution of the variable $\cos\theta_{\gamma_1}$ for signal (blue) and background (orange) for two values of m_a , 5 (left) and 50 (right) GeV.

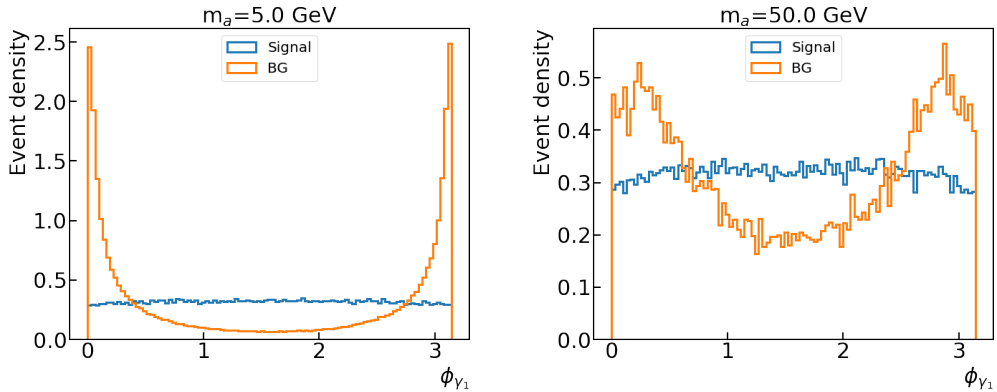


Figure 8. Distribution of the variable ϕ_{γ_1} calculated in the rest frame of the ALP for signal (blue) and background (orange) for two values of m_a , 5 (left) and 50 (right) GeV.

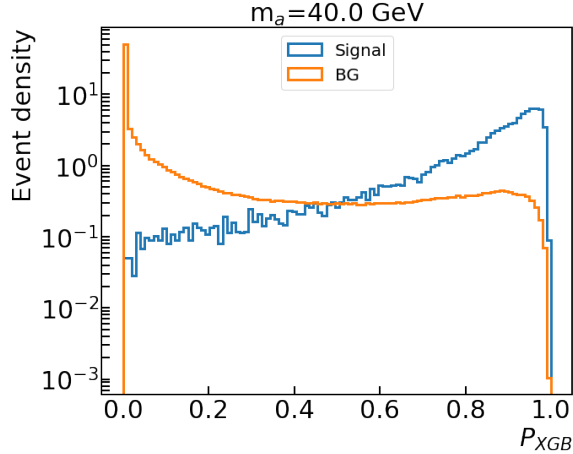


Figure 9. Distribution of the variable P_{XGB} for signal (blue) and background (orange) for $m_a = 40$ GeV.

backgrounds where a particle may have escaped the detector. In addition, loose cuts on the ALP mass kinematics and on the angular distance of the two ALP photons on the face of the calorimeter are applied. These cuts are meant to remove irrelevant events from the training of the selection algorithm, but to retain enough Monte Carlo events in the training and the test samples to ensure a statistically stable selection.

- For the sample thus selected, a boosted decision tree (XGBboost [26]) is trained on five variables, M_{cut} , $E_{\gamma_2}/E_{\gamma_1}$, $\cos\theta_{\gamma_3}$, $\cos\theta_{\gamma_1}$ and ϕ_{γ_1} , where the last two variables are in the rest frame of the (γ_1, γ_2) system.
- Finally a cut on the minimal angular distance between γ_1 and γ_2 in the lab is applied to reject events where the two photons are expected to be merged in the calorimeter, as explained above.
- For a given assumed value of the coupling $C_{\gamma\gamma}$, the number of signal events in the test sample is normalised to the expected statistics of 6×10^{12} Z bosons, and the QED 3-photon background to the target luminosity of 205 ab^{-1} .
- An example of the XGB probability (P_{XGB}) distribution for signal and background is shown in Figure 9, for a 40 GeV test mass. The final cut on P_{XGB} is set at the value optimising the statistical significance Z , defined as in [27]. For a given test mass, Z is calculated for a range of values of $C_{\gamma\gamma}$, and the experimentally accessible region is defined as the $C_{\gamma\gamma}/\Lambda$ interval for which $Z \geq 2$, corresponding to a 95% CL upper limit on the signal strength.

The expected reach in the $(C_{\gamma\gamma}, m_a)$ plane is shown in Figure 10 for the two calorimeter options and for different values of the cut on the $\Delta\alpha$ angle. A significant dependence is observed in both cases for values of m_a below 1 GeV. The performance of the two calorimeter options is compared in Figure 11, for the assumed default values of the selection in $\Delta\alpha$. As expected the crystal calorimeter has a strong advantage where the analysis performance is

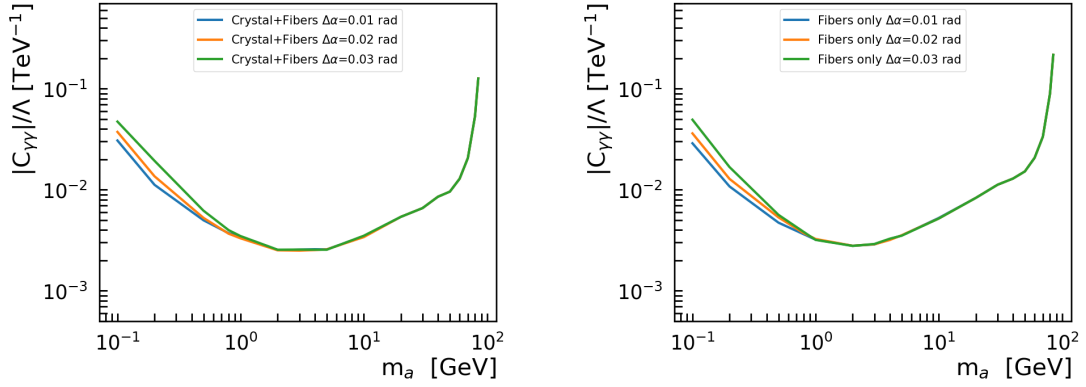


Figure 10. 95% CL sensitivity for the $C_{\gamma\gamma}$ coupling as a function of m_a for the crystal (left) and fibre (right) EM calorimeter. The different curves correspond to different selections on the minimum separation between two photons from the ALP decay applied in the analysis.

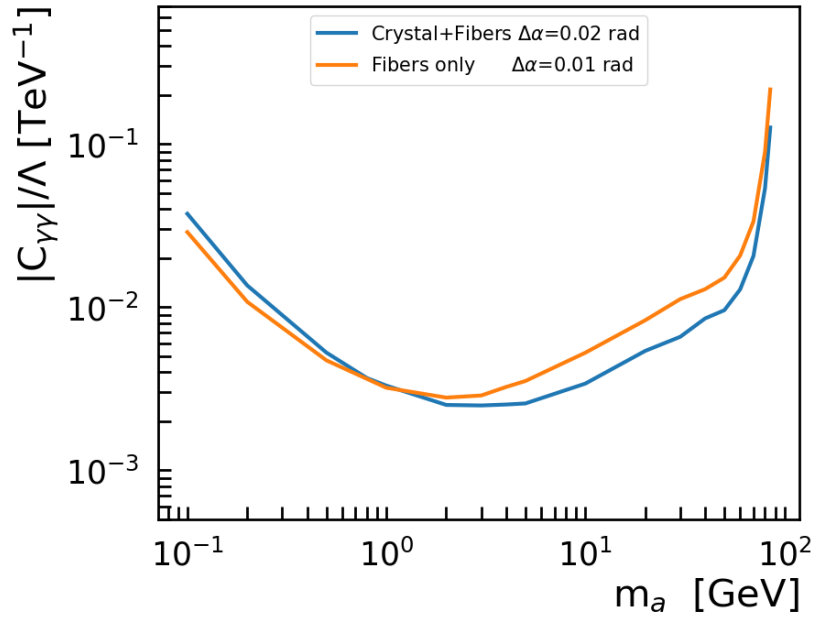


Figure 11. 95% CL sensitivity for the $C_{\gamma\gamma}$ coupling as a function of m_a for the three-photon analysis for the crystal (blue) and fiber (orange) EM calorimeters.

dominated by the photon energy resolution. The impact point resolution is very similar for the two calorimeter options, and the better granularity of the fiber calorimeter is expected to provide better separation power for two very collimated photons. This needs to be confirmed with dedicated full simulation studies which are in progress.

6 Monophoton analysis

The situation in which the ALP decays outside the detector yields a final state with a monochromatic prompt photon recoiling against an invisible particle. This is the monophoton signature, which is a standard way of searching for invisible BSM particles at e^+e^- colliders.

The specificity of the ALP model resides in the fact that the photon is monochromatic, as the invisible particle is produced in the two-body decay of the Z boson, and has an energy very near to the kinematic limit of 45.6 GeV see the recoil formula 5.1, as the values of m_a relevant for the analysis are below 1-2 GeV, as shown in Figure 2.

The θ coverage of the tracking detector of IDEA extends down to 0.15 radians ($|\eta| < 2.6$) from the beam line, whereas the calorimeter extends down to 0.1 radians ($|\eta| < 3$). The experimental topology is therefore the request of a photon within $|\eta| < 2.6$, and no other particle seen in the detector. Two main backgrounds are considered for this analysis:

- the irreducible background is the production of the photon in association with a Z boson which in turn decays invisibly into two neutrinos ($\gamma\nu\nu$ background);
- the main reducible background is the associated production of a photon with two fermions, where both fermions escape the detector. The most important of these backgrounds is the process $e^+e^- \rightarrow \gamma e^+e^-$ which has a very high cross-section for topologies where the two electrons are produced at a small angle from the beam. However, in the kinematic region corresponding to the signal, the radiated photon has to be within the angular acceptance of the inner detector, and carry approximately half of the center-of-mass energy. To balance the transverse momentum of the photon, the associated particles must be produced at a relatively high angle from the beam direction, and thus they have very low probability of escaping the detector unseen.

In order to separate the signal from the background a preselection is applied requiring a single photon with energy in excess of 40 GeV reconstructed in the calorimeter within $|\eta| < 2.6$, no other signal in the calorimeter, and no reconstructed tracks in the inner detector. After this selection the reducible background is fully eliminated, and only the $\gamma\nu\nu$ background survives the selection.

The photon from the Z decay is defined by two variables, its energy, E_γ , and the cosine of its polar angle $\cos\theta_\gamma$. The comparison of signal and background for the two variables is shown in Figure 12. The already powerful rejection which can be obtained by a threshold on the photon energy can be enhanced by a selection on $\cos\theta_\gamma$. The two variables, as for the prompt analysis, are combined using a BDT. A minimum cut on the photon energy of 42 (44.5) GeV is applied for the fiber (crystal) calorimeter respectively before training the

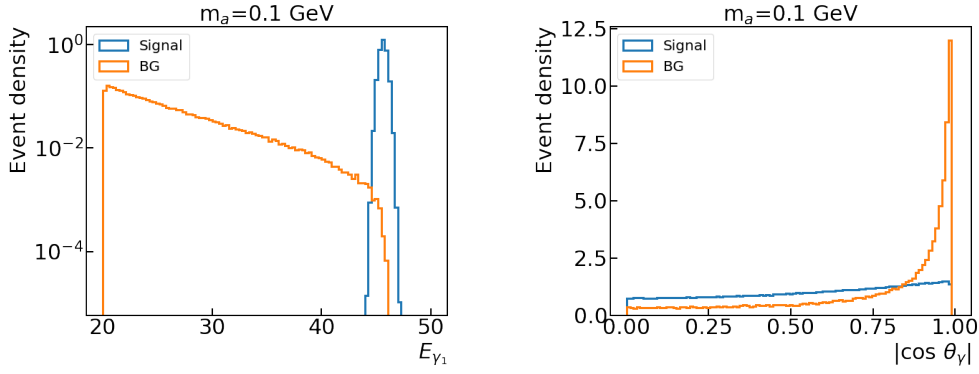


Figure 12. Distribution of the variables E_γ (left) and $\cos\theta_\gamma$ (right) for signal (blue) and background (orange) for $m_a = 1$ GeV.

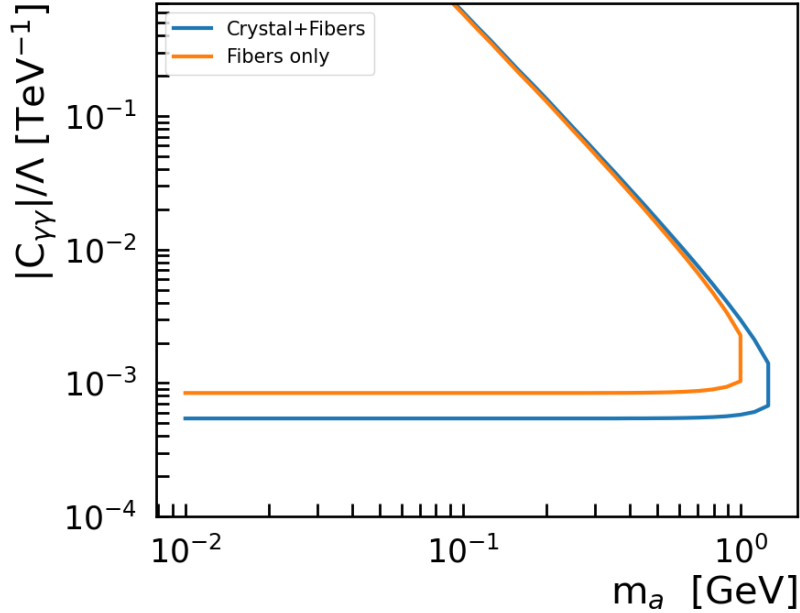


Figure 13. Values the $C_{\gamma\gamma}$ coupling for which the monophoton analysis has a 2σ sensitivity as a function of m_a for the crystal (blue) and fiber (orange) EM calorimeters.

tree. The cut on the output of the tree is chosen to maximise sensitivity for each value of m_a , as explained for the prompt analysis.

The values of the $C_{\gamma\gamma}$ coupling for which this analysis is sensitive to ALP production at 95% CL are shown in Figure 13 for the two calorimeter options as a function of m_a . Given the fact that the background steeply rises with decreasing energy of the photons the much better resolution of the crystal calorimeter yields a significant improvement in coverage.

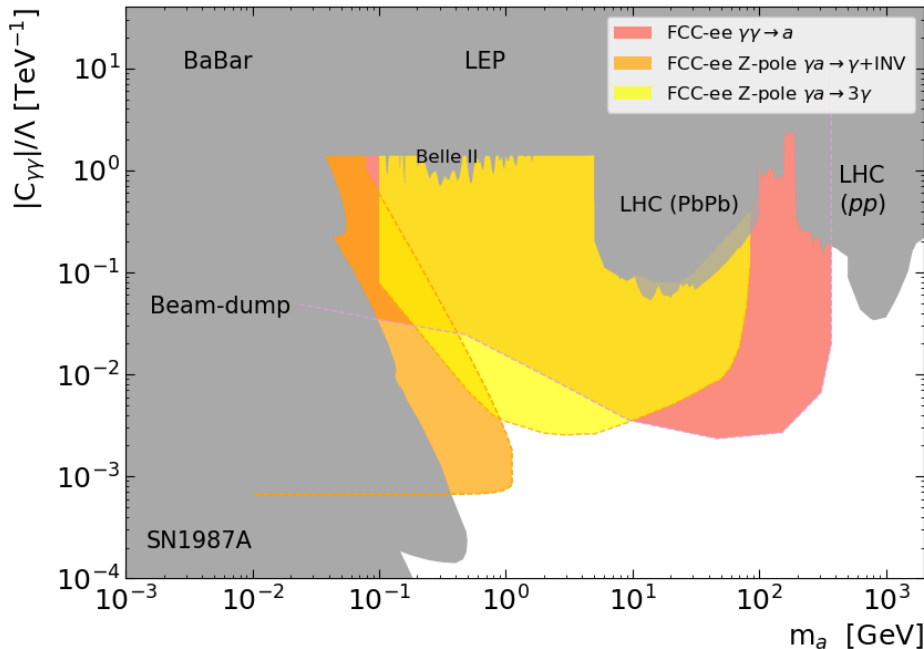


Figure 14. Projected sensitivity for ALPs in the photon coupling versus ALP mass plane from $e^+e^- \rightarrow \gamma a \rightarrow 3\gamma$ analysis (yellow area) and for the $e^+e^- \rightarrow \gamma a \rightarrow \gamma + \text{invisible}$ analysis (orange area) at FCC-ee. The salmon area shows the coverage of the photon-fusion $\gamma\gamma \rightarrow a \rightarrow 2\gamma$ process at FCC-ee from [14]. Other limits are adapted from Ref. [28, 29] updated to the latest LHC results.

7 Combined reach and Conclusions

The Z -pole run at FCC-ee will allow the development of a detailed search program for the decay of a Z boson into a photon and an ALP, with the ALP subsequently decaying into a pair of photons. Depending on the ALP mass and its coupling to the photon and to the Z , different search strategies have been identified, corresponding to different times of flight of the ALP before decaying. A detailed analysis has been performed for a three-photon signal, addressing ALPs which decay inside the detector, and the monophoton search for ALPs decaying outside of the detector. Significant complementary areas of the parameter space are covered by the two analyses. The covered area depends on the energy resolution of the electromagnetic calorimeter, on the resolution on the measurement of the impact position of the photon on the calorimeter, and on how well the invariant mass can be reconstructed when the two photons from the ALP decays are well collimated. Reach curves as a function of these performance parameters have been obtained,

The results of this study are shown in Figure 14, together with the results from [14], compared to existing ALP limits from Ref. [28, 29] updated to the latest LHC results. The three-photon analysis would extend significantly the existing LHC limits in the mass region 1-90 GeV. The monophoton analysis covers the region below 0.1 and 1 GeV which is beyond the reach of the beam dump experiments, and the $\gamma\gamma \rightarrow a$ of Ref. [14] would extend the

mass coverage to $m_a \sim 350$ GeV for comparable values of $C_{\gamma\gamma}$. Thanks to the FCC-ee the complete mass range up to ~ 350 GeV will be explored for couplings larger than a few 10^{-3} TeV $^{-1}$.

References

- [1] A. Abada et al. FCC-ee: The Lepton Collider: Future Circular Collider Conceptual Design Report Volume 2. *Eur. Phys. J. ST*, 228(2):261–623, 2019.
- [2] A. Blondel et al. Searches for long-lived particles at the future FCC-ee. *Front. in Phys.*, 10:967881, 2022.
- [3] Ken Mimasu and Verónica Sanz. ALPs at Colliders. *JHEP*, 06:173, 2015.
- [4] I. Brivio, M. B. Gavela, L. Merlo, K. Mimasu, J. M. No, R. del Rey, and V. Sanz. ALPs Effective Field Theory and Collider Signatures. *Eur. Phys. J. C*, 77(8):572, 2017.
- [5] Martin Bauer, Matthias Neubert, and Andrea Thamm. Collider Probes of Axion-Like Particles. *JHEP*, 12:044, 2017.
- [6] Martin Bauer, Mathias Heiles, Matthias Neubert, and Andrea Thamm. Axion-Like Particles at Future Colliders. *Eur. Phys. J. C*, 79(1):74, 2019.
- [7] Noah Steinberg and James D. Wells. Axion-like particles at the ilc giga-z. *Journal of High Energy Physics*, 2021(8), August 2021.
- [8] M. Antonello. IDEA: A detector concept for future leptonic colliders. *Nuovo Cim. C*, 43(2-3):27, 2020.
- [9] S. Agostinelli et al. GEANT4 - A Simulation Toolkit. *Nucl. Instrum. Meth. A*, 506:250–303, 2003.
- [10] M. Acciarri et al. Search for anomalous $Z \rightarrow \gamma \gamma \gamma$ events at LEP. *Phys. Lett. B*, 345:609–616, 1995.
- [11] M. Z. Akwawy et al. Measurement of the cross-sections of the reactions $e^+ e^- \rightarrow \gamma \gamma$ and $e^+ e^- \rightarrow \gamma \gamma \gamma$ at LEP. *Phys. Lett. B*, 257:531–540, 1991.
- [12] M. Acciarri et al. Tests of QED at LEP energies using $e^+ e^- \rightarrow \gamma \gamma$ (gamma) and $e^+ e^- \rightarrow \text{lepton}^+ \text{lepton}^- \gamma \gamma$. *Phys. Lett. B*, 353:136–144, 1995.
- [13] P. Abreu et al. The reaction $e^+ e^- \rightarrow \gamma \gamma$ (gamma) at Z0 energies. *Phys. Lett. B*, 268:296–304, 1991.
- [14] Patricia Rebello Teles, David d’Enterria, Victor P. Gonçalves, and Daniel E. Martins. Searches for axionlike particles via $\gamma\gamma$ fusion at future e^+e^- colliders. *Phys. Rev. D*, 109(5):055003, 2024.
- [15] Georges Aad et al. Search for nonpointing and delayed photons in the diphoton and missing transverse momentum final state in 8 TeV pp collisions at the LHC using the ATLAS detector. *Phys. Rev. D*, 90(11):112005, 2014.
- [16] Georges Aad et al. Search for displaced photons produced in exotic decays of the Higgs boson using 13 TeV pp collisions with the ATLAS detector. *Phys. Rev. D*, 108(3):032016, 2023.
- [17] J. Alwall, R. Frederix, S. Frixione, V. Hirschi, F. Maltoni, O. Mattelaer, H. S. Shao, T. Stelzer, P. Torrielli, and M. Zaro. The automated computation of tree-level and

next-to-leading order differential cross sections, and their matching to parton shower simulations. *JHEP*, 07:079, 2014.

- [18] Torbjörn Sjöstrand, Stefan Ask, Jesper R. Christiansen, Richard Corke, Nishita Desai, Philip Ilten, Stephen Mrenna, Stefan Prestel, Christine O. Rasmussen, and Peter Z. Skands. An introduction to PYTHIA 8.2. *Comput. Phys. Commun.*, 191:159–177, 2015.
- [19] J. de Favereau, C. Delaere, P. Demin, A. Giammanco, V. Lemaître, A. Mertens, and M. Selvaggi. DELPHES 3, A modular framework for fast simulation of a generic collider experiment. *JHEP*, 02:057, 2014.
- [20] <https://github.com/HEP-FCC/FCC-config/tree/winter2023/FCCee>.
- [21] Andrea Pareti. Exposing a dual-readout fibre calorimeter to electron beams, in preparation for HiDRa: High-resolution calorimeter for e+e- colliders. *Nucl. Instrum. Meth. A*, 1069:169890, 2024.
- [22] Andreas Loeschcke Centeno. Simulation and test beam results of a capillary tube, dual-readout calorimeter. *PoS, ICHEP2024*:1117, 2025.
- [23] Marco T. Lucchini, Lorenzo Pezzotti, Giacomo Polesello, and Christopher G. Tully. Particle flow with a hybrid segmented crystal and fiber dual-readout calorimeter. *JINST*, 17(06):P06008, 2022.
- [24] W. Chung, F. Cetorelli, M. Lucchini, and C. Tully. Full Simulation of a Segmented Crystal ECAL in IDEA. Talk at CALOR 2024, <https://indico.cern.ch/event/1339557/contributions/5898506/>.
- [25] Armen Tumasyan et al. Reconstruction of decays to merged photons using end-to-end deep learning with domain continuation in the CMS detector. *Phys. Rev. D*, 108(5):052002, 2023.
- [26] <https://xgboost.readthedocs.io/en/stable/>.
- [27] ATLAS. Formulae for estimating significance, 2020. ATLAS Note ATL-PHYS-PUB-2020-025 available at <https://cds.cern.ch/record/2736148/files/ATL-PHYS-PUB-2020-025.pdf>.
- [28] Prateek Agrawal et al. Feebly-interacting particles: FIPs 2020 workshop report. *Eur. Phys. J. C*, 81(11):1015, 2021.
- [29] C. Antel et al. Feebly Interacting Particles: FIPs 2022 workshop report. 5 2023.